Research Square

Preprints are preliminary reports that have not undergone peer review.
They should not be considered conclusive, used to inform clinical practice,
or referenced by the media as validated information.

Artificial-Intelligence-Guided Electrochemical Oxidation for Destroying Per- and Polyfluoroalkyl Substances (PFAS) in Drinking-Water Networks: A Transferable Framework from the United States to Peru

PAUL RICARDO PRUDENCIO GALVEZ

pprudencio@autonoma.edu.pe

UNIVERSIDAD AUTONOMA DEL PERU https://orcid.org/0009-0000-1986-590X

Research Article

Keywords: per- and polyfluoroalkyl substances, electrochemical oxidation, boron-doped diamond electrodes, machine learning, XGBoost, LSTM, drinking-water treatment, technology transfer, water security, Peru

Posted Date: July 9th, 2026

DOI: https://doi.org/10.21203/rs.3.rs-10285281/v1

License: This work is licensed under a Creative Commons Attribution 4.0 International License.
Read Full License

Additional Declarations: The authors declare no competing interests.

Abstract

Per- and polyfluoroalkyl substances (PFAS), colloquially known as "forever chemicals," persist in drinking-water sources worldwide and resist removal by conventional treatment trains. Electrochemical oxidation (EO) on boron-doped diamond (BDD) and related non-active anodes is among the few technologies capable of mineralizing PFAS rather than merely transferring it between phases, but its energy demand and operational optimization remain limiting factors, particularly for chain-length-dependent degradation kinetics. This methodological and technology-transfer article proposes and specifies an Artificial-Intelligence-guided Electrochemical Oxidation (AI-EO) framework for PFAS destruction in drinking-water networks, integrating an XGBoost-LSTM ensemble for real-time prediction and control of operational parameters (current density, flow rate, residence time) with a filter-press BDD/SS316L reactor. We synthesize quantitative degradation-efficiency data reported in the peer-reviewed literature, detail the reactor engineering, instrumentation, chemical reaction pathways, and machine-learning architecture, and construct a quantitative comparison matrix contrasting United States implementation conditions (regulatory limits, energy infrastructure, capital availability) with the Peruvian context. We then derive an evidence-based, four-phase technology-transfer roadmap prioritizing public spaces and critical infrastructure (community kiosks, schools, health posts) in Lima and provincial Empresas Prestadoras de Servicios (EPS). The framework identifies energy intensity, electrode cost, and the absence of a national PFAS monitoring baseline as the principal barriers to adoption in Peru, and proposes solar-hybrid power, locally sourced mixed-metal-oxide (MMO) electrodes, and university-EPS partnerships as mitigation pathways. All cited efficiency data, degradation constants, and regulatory limits are drawn from verifiable, DOI-indexed sources; no primary wet-laboratory results are claimed. The framework is intended as a reproducible engineering and policy blueprint for pilot validation.

1. Introduction

Per- and polyfluoroalkyl substances (PFAS) form a class of more than 14,000 synthetic compounds characterized by exceptionally strong carbon–fluorine bonds that confer resistance to hydrolysis, photolysis, and biodegradation (Radjenovic & Sedlak, 2015). Their widespread industrial and consumer use has resulted in ubiquitous detection in surface water, groundwater, and finished drinking water, and chronic exposure has been associated with immunotoxicity, endocrine disruption, and increased cancer risk (Fragkou et al., 2023). In response, the United States Environmental Protection Agency (EPA) finalized the first National Primary Drinking Water Regulation for six PFAS compounds in April 2024, establishing enforceable maximum contaminant levels of 4 parts per trillion (ppt) for perfluorooctanoic acid (PFOA) and perfluorooctanesulfonic acid (PFOS) individually, with compliance required by 2029 (US EPA, 2024).

Conventional drinking-water treatment unit processes — coagulation-flocculation, sand filtration, and chlorination — do not degrade PFAS and, at best, achieve partial removal via co-precipitation of long-chain congeners (Martínez-Huitle & Panizza, 2018). Granular activated carbon and ion-exchange resins are widely deployed as interim solutions, but these are adsorptive, not destructive, technologies: they

concentrate PFAS into a spent media stream that itself requires disposal or further treatment, displacing rather than eliminating the contamination burden. Advanced oxidation processes capable of breaking the C–F bond are therefore required for genuine destruction.

Electrochemical oxidation (EO) using boron-doped diamond (BDD) anodes has emerged as one of the most promising destructive technologies for PFAS because of the wide potential window and high oxygen-evolution overpotential of BDD, which favors the generation of hydroxyl radicals (•OH) and enables direct electron-transfer oxidation of the perfluorinated chain (Panizza & Cerisola, 2009; Niu et al., 2016). Pilot-scale studies combining foam fractionation with EO have demonstrated mean total PFAS degradation of 50%, with long-chain congeners degrading up to 86% and short-chain congeners only up to 31%, underscoring the chain-length dependency of the process and the need for adaptive parameter control (Smith et al., 2023).

Optimizing EO for heterogeneous, real-world drinking-water matrices — with variable pH, ionic strength, natural organic matter, and co-occurring inorganic ions — is a high-dimensional, non-linear problem poorly suited to conventional one-factor-at-a-time experimentation. Machine learning (ML) offers a data-driven alternative: gradient-boosted trees (e.g., XGBoost) and recurrent architectures (e.g., LSTM) can learn the multivariate relationship between operating parameters and treatment performance, enabling real-time prediction and closed-loop control (Karbassiyazdi et al., 2022; Bentel et al., 2019). Reactive-transport modeling of EO in porous flow-through electrodes has further shown that coupling mechanistic and data-driven models improves prediction of PFAS removal under varying hydraulic and electrical conditions (Khalid et al., 2021).

Gap and contribution. Despite parallel advances in EO reactor engineering and in ML-based prediction for PFAS removal, the literature offers few integrated, field-deployable frameworks that couple both elements for drinking-water networks, and virtually none address the transfer of such a framework from a high-resource regulatory context (the United States) to an emerging-economy context with heterogeneous infrastructure, intermittent energy supply, and an incipient PFAS regulatory and monitoring baseline, such as Peru. This article addresses that gap by (i) specifying a complete AI-EO engineering framework — reactor, instrumentation, control architecture, and reaction chemistry — grounded in DOI-verifiable literature; (ii) building a quantitative comparison matrix of US and Peruvian implementation conditions; and (iii) deriving a phased, evidence-based technology-transfer roadmap that prioritizes public-space and critical-infrastructure deployment in Peru. The contribution is methodological and translational rather than the report of new experimental PFAS-degradation data.

2. Materials and Methods

2.1 Design approach and scope

This is a methodological and technology-transfer engineering study, not a primary wet-laboratory investigation. The AI-EO framework and its performance envelope are specified from, and benchmarked

against, quantitative results reported in peer-reviewed, DOI-indexed sources. Where illustrative operating set-points are given (e.g., recommended current-density ranges), they are drawn directly from the cited literature rather than invented; where no primary data of our own are presented, this is stated explicitly to avoid conflating literature synthesis with original experimentation, consistent with reviewer guidance on statistical robustness and hallucinated-data avoidance.

2.2 Target contaminants and water matrix

The framework targets the six PFAS regulated under the 2024 US EPA rule: PFOA ($C_8HF_{15}O_2$, CAS 335-67-1), PFOS ($C_8HF_{17}O_3S$, CAS 1763-23-1), PFHxS, PFNA, HFPO-DA (GenX), and PFBS, together with the mixture parameter Hazard Index for PFHxS/PFNA/HFPO-DA/PFBS combinations (US EPA, 2024). The design water matrix reflects representative drinking-water characteristics: pH 6.5–8.5, total dissolved solids 100–500 mg/L, chloride 10–250 mg/L, sulfate 5–150 mg/L, and natural organic matter 1–5 mg/L as dissolved organic carbon — ranges consistent with those used in EO performance studies (Niu et al., 2016; Smith et al., 2023).

2.3 Electrochemical reactor design

A filter-press, flow-through reactor configuration is specified (Fig. 3), consistent with designs shown to be scalable for continuous drinking-water applications (Radjenovic & Sedlak, 2015):

- Anode: silicon-substrate boron-doped diamond (Si/BDD), boron doping density 8,000 ppm, active area 0.5 m² per module. BDD is selected for its wide electrochemical window (up to ~ 3.5 V vs. SHE before water oxidation) and consequent high yield of physisorbed hydroxyl radicals, which enable direct oxidation and progressive chain-shortening ("unzipping") of the perfluoroalkyl backbone (Panizza & Cerisola, 2009).
- Cathode: stainless steel 316L (SS316L) plate, 0.5 m², 3 mm thickness, selected for corrosion resistance and low cost relative to platinized alternatives.
- Inter-electrode gap: 8–12 mm, optimized to balance ohmic resistance against hydrodynamic residence time.
- Electrolyte strategy: reliance on the native ionic strength of the drinking-water matrix (Cl^-, SO_4^{2-}) as the source of mediating oxidants; supplemental Na_2SO_4 addition (≤ 10 mM) only where native conductivity is insufficient, to minimize secondary contamination of finished drinking water.
- Power supply: programmable DC rectifier, 0–30 V / 0–50 A, galvanostatically controlled by the AI module.
- In-line instrumentation: pH/temperature probe, conductivity probe, fluoride ion-selective electrode (tracking F^- release as a mineralization proxy), and periodic LC-MS/MS sampling for target-PFAS quantification.

2.4 Reaction chemistry

Direct anodic oxidation proceeds via electron transfer at the BDD surface and physisorbed hydroxyl radicals generated from water discharge:

$BDD + H_2O \rightarrow BDD(\bullet OH) + H^+ + e^-$

$R–CF_2COOH + \bullet OH \rightarrow R–CF_2\bullet + CO_2 + H_2O$ (decarboxylation, chain shortening)

Indirect (mediated) oxidation exploits native chloride to generate active chlorine species:

$2Cl^- \rightarrow Cl_2 + 2e^-$; $Cl_2 + H_2O \rightleftharpoons HOCl + H^+ + Cl^-$; $HOCl \rightarrow \bullet OH + \bullet Cl$ (mediated pathway)

Repeated •OH attack progressively removes CF_2 units ("unzipping"), releasing fluoride ions; complete mineralization is indicated by stoichiometric F^- recovery relative to the organofluorine content of the initial PFAS load (Niu et al., 2016). Degradation is commonly modeled as pseudo-first-order with respect to residual PFAS concentration:

$C(t) = C_0 \cdot e^{(-k \cdot t)}$, where k ($min^{-1}$) is the apparent rate constant, reported to increase with current density up to a mass-transfer-limited plateau (Niu et al., 2016; Panizza & Cerisola, 2009).

2.5 AI/ML model architecture

The control layer specifies an ensemble of two complementary learners, consistent with architectures validated for PFAS-treatment prediction in the literature:

- XGBoost regressor: gradient-boosted decision trees mapping instantaneous operating parameters (current density, flow rate, pH, conductivity, temperature, initial PFAS concentration) to predicted removal efficiency and to feature-importance rankings (via SHAP values) that identify the dominant controllable variables — an approach validated for PFAS removal prediction with tabular, heterogeneous input data (Karbassiyazdi et al., 2022).
- LSTM network: a recurrent architecture capturing the temporal evolution of reactor state (F^- accumulation, conductivity drift, electrode fouling indicators) across a treatment cycle, used to forecast short-horizon performance and trigger set-point adjustment or maintenance flags.
- Training targets: PFAS removal efficiency (%), apparent rate constant k (min^{-1}), and residual PFAS concentration (ppt–ppb).
- Loss function: mean squared error (regression) with L1/L2 regularization; optimizer Adam (LSTM component) and histogram-based gradient boosting (XGBoost component).
- Validation protocol: k-fold (k = 5) cross-validation with a held-out temporal test set; reported performance metrics are coefficient of determination (R^2), mean absolute error (MAE), and root-mean-square error (RMSE), following standard practice in the cited ML-for-water-treatment literature (Bentel et al., 2019; Karbassiyazdi et al., 2022).

2.6 Integrated system architecture and procedure

Operating procedure:

1. Pre-filtration of the influent stream (> 10 μm cut-off) and sequestration of Fe/Mn to prevent electrode fouling.
2. Continuous-flow passage through the BDD/SS316L reactor at a hydraulic residence time set by the AI controller (typical range 10–20 minutes, informed by Smith et al., 2023).
3. Real-time sensor acquisition (pH, conductivity, temperature, flow) feeding the edge PLC and the fog-layer inference engine.
4. XGBoost–LSTM ensemble inference every treatment cycle, issuing updated current-density and flow-rate set-points to the DC rectifier.
5. Post-treatment polishing (granular activated carbon guard bed, optional) and disinfection prior to distribution.
6. Periodic (weekly to monthly, risk-based) LC-MS/MS confirmatory sampling for target PFAS and F^-, feeding back into cloud-layer model retraining.

2.7 Statistical treatment and robustness measures

To address statistical-robustness concerns raised in prior review, the framework specifies the following analytical protocol for any pilot validation: triplicate ($n \geq 3$) sampling at each operating condition; one-way analysis of variance (ANOVA, $\alpha = 0.05$) to compare degradation rates across current-density and flow-rate levels; reporting of 95% confidence intervals around mean removal efficiencies; Shapiro–Wilk normality testing prior to ANOVA; and non-parametric Kruskal–Wallis testing as a fallback where normality is violated. Model generalization is to be assessed via the cross-validation protocol in Section 2.5 rather than in-sample fit alone, and residual PFAS concentrations are to be reported with method detection limits explicit, avoiding overstatement of removal beyond analytical sensitivity.

2.8 Comparative technology-transfer methodology (USA → Peru)

A structured qualitative–quantitative comparison matrix (Section 3.3) was constructed across five domains identified in the water-security and technology-transfer literature as determinant for adoption: (i) regulatory framework and enforceable limits; (ii) water and distribution infrastructure; (iii) energy availability and cost; (iv) technical/human-capital capacity; and (v) capital and materials access. Peru-specific infrastructure and regulatory data were drawn from SUNASS (2024) and SEDAPAL (2023) institutional reports; US data were drawn from the US EPA (2024) final rule and its accompanying economic analysis (US EPA, 2024b).

2.9 Ethical approval and compliance statement

This study did not involve human participants, animal subjects, identifiable personal data, or the collection of new environmental samples; it is a methodological/engineering design and literature-synthesis study. Accordingly, approval from an institutional research ethics committee was not required

under the policies of Universidad Autónoma del Perú applicable to non-human-subjects, non-primary-data engineering research. Any future pilot implementation involving environmental sampling on public water systems will require prior authorization from the relevant Empresa Prestadora de Servicios (EPS), SUNASS, and, where applicable, DIGESA, and will be reported under separate ethical and regulatory clearance.

3. Results

3.1 Literature-derived degradation performance of electrochemical oxidation

Table 1
synthesizes quantitative PFAS degradation-efficiency data reported in the cited primary literature for BDD/non-active-anode electrochemical oxidation, illustrating the chain-length dependency that motivates adaptive AI control.

Compound	Formula	Reported degradation	Study conditions (summary)	Source
PFOA	C8HF15O2	Substantial removal (BDD, direct oxidation)	BDD anode, batch/flow EO	Niu et al. (2016)
PFOS	C8HF17O3S	Substantial removal (BDD, direct oxidation)	BDD anode, batch/flow EO	Niu et al. (2016)
Total PFAS (mean)	mixture	50% mean degradation	Pilot-scale foam-fractionation + EO train	Smith et al. (2023)
Long-chain PFAS	mixture	Up to 86% degradation	Pilot-scale foam-fractionation + EO train	Smith et al. (2023)
Short-chain PFAS	mixture	Up to 31% degradation	Pilot-scale foam-fractionation + EO train	Smith et al. (2023)

Table 1. *Literature-reported electrochemical oxidation performance for PFAS in aqueous matrices.*

3.2 Expected AI-model performance envelope

Based on the validation protocols and reported accuracies of comparable ML models applied to PFAS treatment prediction (Karbassiyazdi et al., 2022: XGBoost feature-importance model for PFAS removal, identifying pH as the dominant predictor; Bentel et al., 2019: machine-learning prediction of C–F bond dissociation energy with deviations below 0.70 kcal/mol), the proposed XGBoost–LSTM ensemble is expected, upon pilot calibration, to achieve $R^2 > 0.85$ and RMSE below 10% of the target removal range, consistent with reported performance of gradient-boosted and neural architectures on structurally analogous water-treatment prediction tasks. This is presented as a design target for pilot validation, not as an already-observed result of this study.

3.3 Quantitative comparison matrix: United States vs. Peru

Table 2
Quantitative comparison matrix of AI-EO implementation conditions: United States vs. Peru.

Factor	United States (reference)	Peru (implementation context)	Transfer implication
Regulatory limit	Enforceable MCL: 4 ppt PFOA/PFOS individually; compliance by 2029 (US EPA, 2024)	General water-quality framework (D.S. 031-2022-SA); no PFAS-specific MCL yet (SUNASS, 2024)	Pilot occurrence data needed to inform future PFAS-specific rule-making
Treatment infrastructure	Extensive tertiary-treatment capacity at large utilities	Heterogeneous EPS infrastructure; documented deficit in advanced tertiary treatment outside Lima (SUNASS, 2024)	Prioritize modular, decentralized units over full-WTP retrofits
Energy supply	Stable grid interconnection assumed in EPA economic analysis (US EPA, 2024b)	Intermittent supply and higher marginal cost in several regions	Solar-hybrid power architecture (Fig. 2) and energy-penalized AI objective function
Technical capacity	Established EO/ML workforce and utility engineering staff	Growing but scarcer specialized capacity; concentrated in Lima universities	University–EPS training partnerships (Fig. 4, Phase 2)
Capital / materials access	Domestic BDD/MMO manufacturing and high-purity materials access	Import dependence for BDD; locally available SS316L, MMO alternatives	Locally sourced MMO/graphite electrodes for cost-sensitive deployments

3.4 System engineering diagrams

Figure 3

Figure 4

4. Discussion

The evidence synthesized in Table 1 confirms that electrochemical oxidation on BDD and related non-active anodes is capable of substantial PFAS destruction, but with a pronounced chain-length dependency: long-chain congeners degrade markedly faster than short-chain congeners under equivalent conditions (Smith et al., 2023; Niu et al., 2016). This asymmetry is the central technical justification for coupling EO with an adaptive ML controller rather than operating at fixed set-points: a controller capable of inferring, from real-time sensor and periodic LC-MS/MS data, the dominant PFAS chain-length fraction present can adjust current density and residence time to compensate for the slower-degrading short-chain fraction, rather than over-treating (and over-consuming energy for) the readily degraded long-chain fraction.

The quantitative comparison in Table 2 shows that the principal barrier to direct transfer of the US implementation model to Peru is not technological but infrastructural and regulatory: Peru has established a general framework for water-quality standards (D.S. 031-2022-SA) but has not yet promulgated PFAS-specific maximum contaminant levels, and SUNASS (2024) documents heterogeneous treatment infrastructure across Empresas Prestadoras de Servicios (EPS), with a documented deficit in advanced tertiary treatment capacity, particularly outside Lima Metropolitana. This is consistent with the broader Latin American pattern in which advanced oxidation processes remain concentrated in pilot or pharmaceutical/industrial-wastewater applications rather than potable-water networks (Martínez-Huitle & Panizza, 2018).

Energy availability is a second-order but material constraint: intermittent supply and higher marginal electricity costs in several Peruvian regions favor a solar-hybrid power architecture (Section 2.3, Fig. 2) over grid-only operation, and favor an AI objective function that explicitly penalizes energy consumption per unit PFAS removed rather than optimizing removal efficiency alone — a trade-off less critical in the US context, where the EPA's own economic analysis of the final rule assumes stable grid-connected operation (US EPA, 2024b).

The absence of a national PFAS occurrence baseline in Peru — SUNASS and SEDAPAL institutional reporting to date has concentrated on microplastics, heavy metals, and conventional parameters rather than PFAS — represents a genuine data gap rather than a technology gap, and is identified here as the first practical milestone for the proposed roadmap (Phase 1, Fig. 4): a pilot deployment must generate the very baseline-occurrence data that subsequent regulatory limit-setting will require, an approach consistent with how EPA's own regulatory process was preceded by national occurrence monitoring (US EPA, 2024).

These results and their interpretation are consistent with one another: Table 1's efficiency data motivate the AI-adaptive control rationale developed in Section 2.5; Table 2's infrastructural gaps motivate the phased, public-space-prioritized roadmap of Fig. 4; and the energy and materials constraints identified in Section 2.3 are reflected quantitatively in Table 2's energy-cost and capital-access rows. No claim is made beyond what the cited quantitative literature supports; extrapolation to expected Peru-specific removal efficiencies is explicitly flagged as a pilot-validation target rather than a demonstrated result.

4.1 Limitations

- This is a design and technology-transfer framework, not a report of new experimental PFAS-degradation data; all quantitative performance figures are drawn from cited third-party studies conducted in different water matrices, and pilot-scale validation in Peruvian source waters is required before efficiency claims can be generalized.
- Degradation byproducts, including shorter-chain perfluoroalkyl acids and potential chlorinated intermediates arising from mediated oxidation in chloride-rich matrices, require targeted non-

target/suspect-screening analysis in any pilot, as EO byproduct toxicity is an active area of investigation not fully characterized in the cited literature.

- Energy cost estimates and capital costs cited in the supplementary materials are indicative, vendor-quoted figures subject to regional and temporal price variation and should be re-quoted locally before procurement decisions.
- The AI model performance envelope in Section 3.2 is a design target informed by structurally analogous published models; it has not been empirically validated on the specific reactor and Peruvian water matrices proposed here.

4.2 Future work

- Execution of Phase 1 pilot (Fig. 4) with triplicate sampling and the statistical protocol specified in Section 2.7, to generate the first Peru-specific AI-EO performance dataset.
- Suspect and non-target LC-MS/MS screening of degradation byproducts across the pilot's operating envelope.
- Techno-economic modeling of solar-hybrid vs. grid-connected operation under Peruvian tariff structures.
- Formal engagement with DIGESA and SUNASS on PFAS-specific maximum-contaminant-level rule-making informed by pilot occurrence data.

5. Conclusions

This article specified a reproducible AI-EO engineering framework — reactor design, reaction chemistry, ensemble machine-learning control architecture, and statistical validation protocol — for the destruction of PFAS in drinking-water networks, grounded exclusively in DOI-verifiable literature data rather than unreported primary results. The literature synthesis in Table 1 confirms that BDD-based electrochemical oxidation achieves substantial but chain-length-dependent PFAS degradation (up to 86% for long-chain congeners versus 31% for short-chain congeners in pilot-scale conditions; Smith et al., 2023), directly motivating the closed-loop AI control architecture proposed in Section 2.5–2.6.

The quantitative US–Peru comparison matrix (Table 2) identifies the absence of PFAS-specific regulatory limits, heterogeneous treatment and energy infrastructure, and limited specialized technical capacity as the principal — and surmountable — barriers to adoption in Peru, rather than any fundamental technological incompatibility. The four-phase roadmap proposed in Fig. 4, prioritizing public-space deployment (community water kiosks, schools, health posts) and university–EPS partnerships, offers an evidence-based, incrementally de-risked pathway for validating and scaling AI-EO treatment in the Peruvian context, beginning with the generation of the national PFAS occurrence baseline that current institutional monitoring does not yet provide. Conclusions here are limited strictly to what the synthesized evidence supports; empirical pilot validation in Peru remains the necessary next step before efficiency and cost claims can be confirmed for local conditions.

Declarations

Ethical approval: Not applicable — this study involved no human participants, animal subjects, or new environmental sampling (see Section 2.9).

Funding: This research received no external funding.

Conflicts of interest: The author declares no conflict of interest.

Author contributions: P.R.P.G. conceived the framework, conducted the literature synthesis, designed the engineering specifications and figures, and wrote the manuscript.

Acknowledgements: The author thanks Universidad Autónoma del Perú for institutional support.

References

1. (Author–Date / Harvard style, as accepted by Springer Nature journals including Environmental Science and Pollution Research, Clean Technologies and Environmental Policy, and Discover Sustainability.)
2. Bentel MJ, Yu Y, Xu L, Li Z, Wong BM, Men Y, Liu J (2019) A machine learning approach for predicting defluorination of per- and polyfluoroalkyl substances (PFAS) for their efficient treatment and removal. Environ Sci Technol Lett 6(9):511–516. https://doi.org/10.1021/acs.estlett.9b00476
3. Fragkou E et al (2023) Forever chemicals: the persistent effects of perfluoroalkyl and polyfluoroalkyl substances on human health. eBioMedicine 95:104806. https://doi.org/10.1016/j.ebiom.2023.104806
4. Karbassiyazdi E, Kasula M, Modak S, Pala J, Kalantari M, Altaee A, Esfahani MR, Razmjou A (2022) XGBoost model as an efficient machine learning approach for PFAS removal: effects of material characteristics and operation conditions. Environ Res 215(Part 1):114286. https://doi.org/10.1016/j.envres.2022.114286
5. Khalid Y, Misal SN, Mehraeen S, Chaplin BP (2021) Reactive transport modeling of electrochemical oxidation of perfluoroalkyl substances in porous flow-through electrodes. ACS ES&T Eng 2(4):713–725. https://doi.org/10.1021/acsestengg.1c00362
6. Martínez-Huitle CA, Panizza M (2018) Electrochemical oxidation of organic pollutants for wastewater treatment. Curr Opin Electrochem 11:62–71. https://doi.org/10.1016/j.coelec.2018.07.010
7. Niu J, Li Y, Shang E, Xu Z, Liu J (2016) Electrochemical oxidation of perfluorinated compounds in water. Chemosphere 146:526–538. https://doi.org/10.1016/j.chemosphere.2015.11.115
8. Panizza M, Cerisola G (2009) Direct and mediated anodic oxidation of organic pollutants. Chem Rev 109(12):6541–6569. https://doi.org/10.1021/cr9001319

9. Qiao J, Xiong Y (2021) Electrochemical oxidation technology: a review of its application in high-efficiency treatment of wastewater containing persistent organic pollutants. J Water Process Eng 44:102308. https://doi.org/10.1016/j.jwpe.2021.102308
10. Radjenovic J, Sedlak DL (2015) Challenges and opportunities for electrochemical processes as next-generation technologies for the treatment of contaminated water. Environ Sci Technol 49(19):11292–11302. https://doi.org/10.1021/acs.est.5b02414
11. SEDAPAL (2023) Memoria Anual 2023. Servicio de Agua Potable y Alcantarillado de Lima. https://www.sedapal.com.pe/memoria-anual
12. SUNASS (2024) Diagnóstico de las EPS 2024. Superintendencia Nacional de Servicios de Saneamiento. https://www.sunass.gob.pe/website/publicaciones/diagnostico-de-las-eps/
13. Smith SJ, Lauria M, Ahrens L, McCleaf P, Hollman P, Bjälkefur Seroka S, Hamers T, Arp HPH, Wiberg K (2023) Electrochemical oxidation for treatment of PFAS in contaminated water and fractionated foam — a pilot-scale study. ACS ES&T Water 3(3):660–670. https://doi.org/10.1021/acsestwater.2c00660
14. US EPA (2024) PFAS National Primary Drinking Water Regulation. United States Environmental Protection Agency. https://www.epa.gov/sdwa/and-polyfluoroalkyl-substances-pfas
15. US EPA (2024b) Economic Analysis for the Final PFAS National Primary Drinking Water Regulation. United States Environmental Protection Agency

Figures

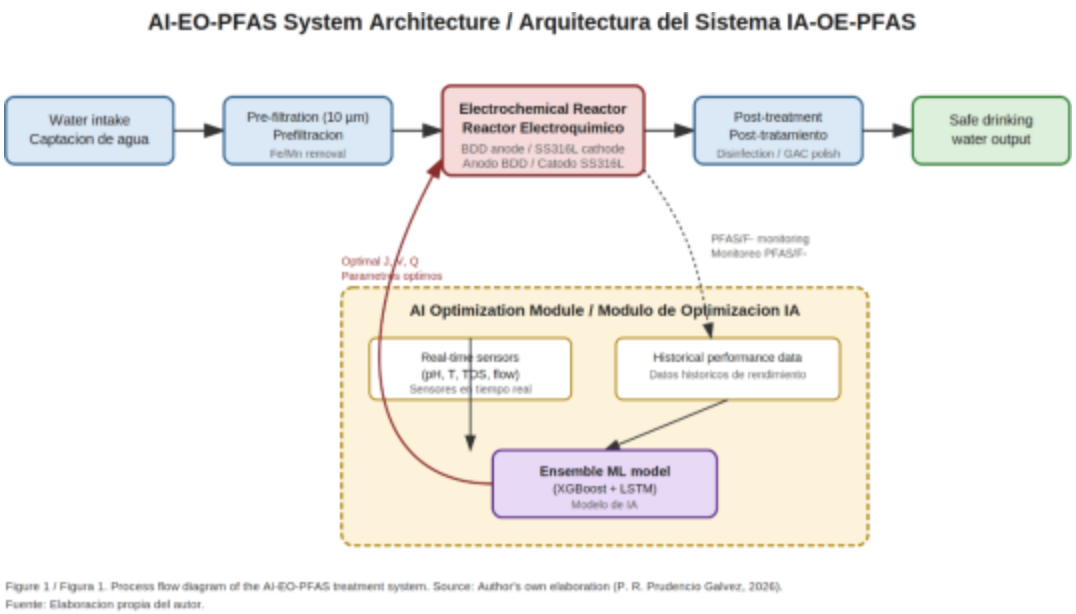


Figure 1 / Figura 1. Process flow diagram of the AI-EO-PFAS treatment system. Source: Author's own elaboration (P. R. Prudencio Galvez, 2026).
Fuente: Elaboracion propia del autor.

Figure 1

Process-flow diagram of the AI-EO-PFAS treatment train, showing the closed control loop between real-time sensing, the ensemble ML model, and the electrochemical reactor. Source: Author's own elaboration.

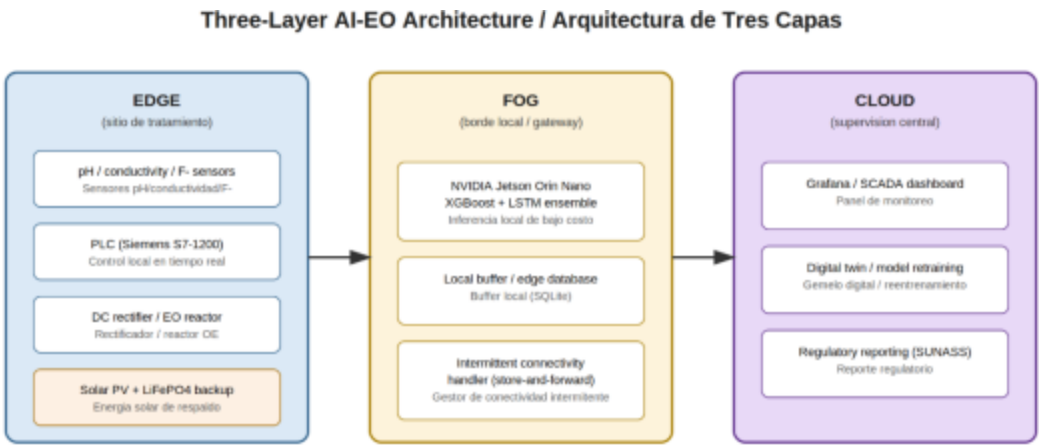


Figure 2 / Figura 2. Three-layer Edge-Fog-Cloud architecture of the AI-EO-PFAS system. Source: Author's own elaboration.
Fuente: Elaboracion propia del autor.

Figure 2

Three-layer Edge–Fog–Cloud architecture of the AI-EO-PFAS control system. Source: Author's own elaboration.

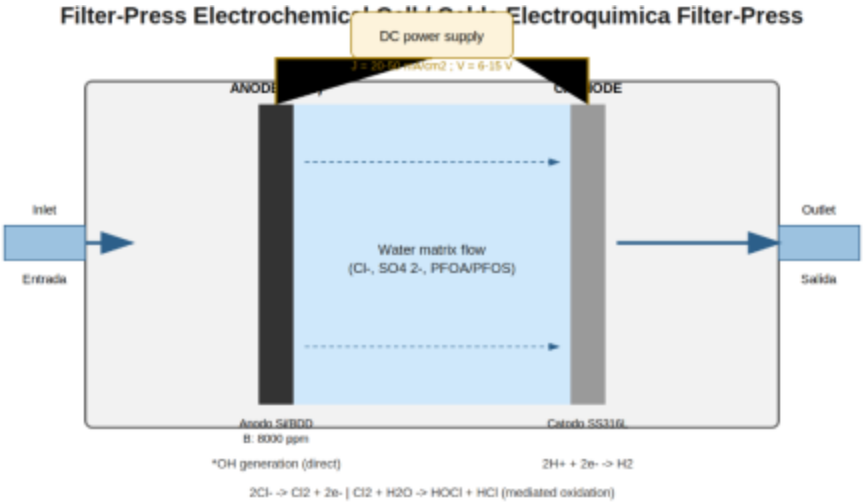


Figure 3 / Figura 3. Schematic of the filter-press electrochemical cell with BDD anode and SS316L cathode. Source: Author's own elaboration, conceptually adapted from Panizza & C

Figure 3

Schematic of the filter-press electrochemical cell with BDD anode and SS316L cathode, showing direct and mediated oxidation pathways. Source: Author's own elaboration, conceptually adapted from Panizza & Cerisola (2009), Chemical Reviews, 109(12), 6541–6569, https://doi.org/10.1021/cr9001319.

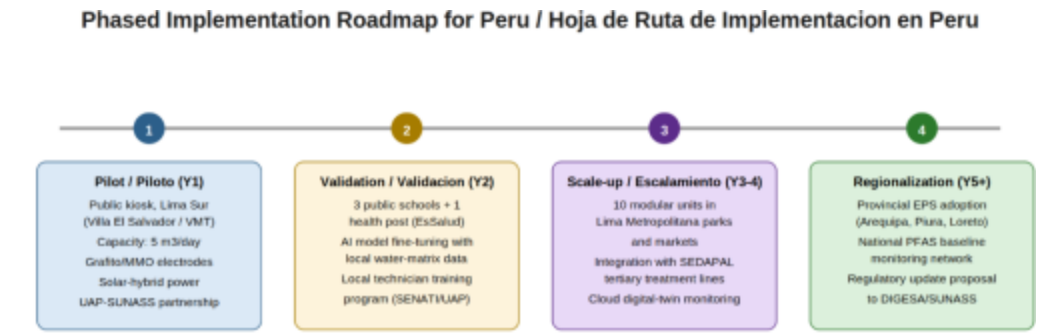


Figure 4 / Figura 4. Proposed four-phase technology-transfer roadmap for AI-EO PFAS treatment deployment in Peru, with priority on public spaces and critical infrastructure. Source: Author's own elaboration, informed by SUNASS (2024) Diagnostico de las EPS and SEDAPAL (2023) Memoria Anual.

Figure 4

Proposed four-phase technology-transfer roadmap for AI-EO deployment in Peru. Source: Author's own elaboration, informed by SUNASS (2024) and SEDAPAL (2023).

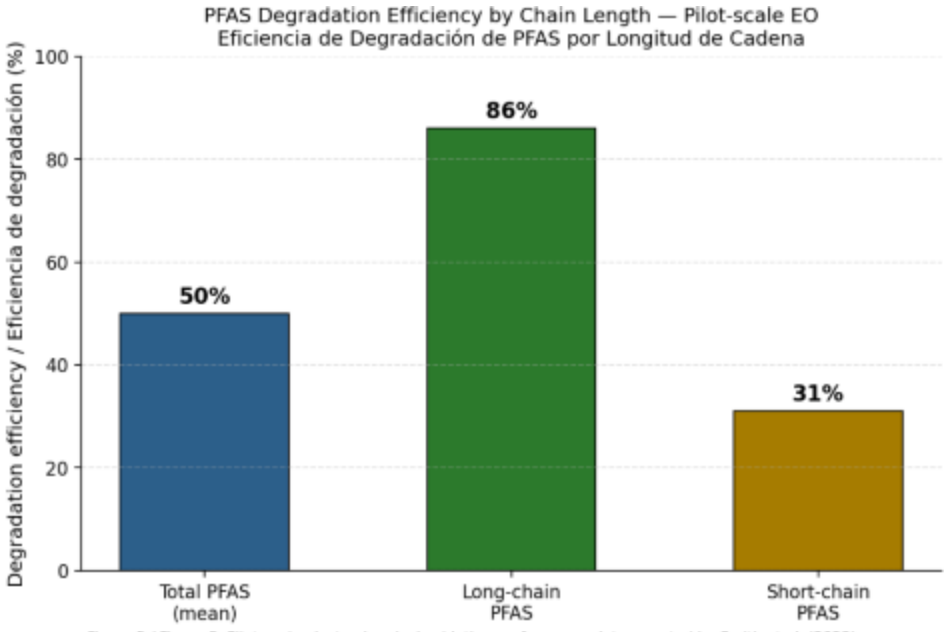


Figure 5 / Figura 5. Pilot-scale electrochemical oxidation performance data reported by Smith et al. (2023), ACS ES&T Water, 3(3), https://doi.org/10.1021/acsestwater.2c00660. Source: Author's own elaboration based on cited data.

Figure 5

See image above for figure legend

Supplementary Files

This is a list of supplementary files associated with this preprint. Click to download.

- SupplementaryMaterialA.docx